Proceedings of the 1990 ASME International Computers in Engineering Conference,
ASME Book No. G0515B, Vol. II, August, 1990.

MULTI-RIGID-BODY KINEMATIC ANALYSIS WITH ELASTIC FINITE ELEMENTS

J. W. Eischen (Assistant Professor)
H. K. Sun (Graduate Student)
M. E. Marler (Graduate Student)
Department of Mechanical and Aerospace Engineering
North Carolina State University
Raleigh, NC 27695

ABSTRACT

The purpose of this paper is to show how kinematic analysis of certain multi-rigid-body systems may be accomplished by discretization with finite elements having extensional, bending, and shear flexibilities. The novel feature of the method is that kinematic analysis of multi-rigid-body systems is treated in a manner completely consistent with multi-flexible-body systems. Several numerical simulations are presented dealing with planar mechanisms composed of slender links connected by revolute and/or prismatic joints .

INTRODUCTION

Kinematics is the study of the position, velocity, and acceleration of points on bodies that make up a mechanical system. Angular velocities and accelerations are also of interest if the bodies are rigid. Kinematic analysis is independent of the forces that may be acting on the system. Traditional kinematic analysis of a mechanical system comprised of many rigid mechanical elements begins by selecting a set of coordinates to describe the position and orientation of the individual bodies. The four-bar linkage treated in many textbooks is a classic example of a multi-rigid-body system. Next, constraint equations are formulated, usually having to do with restrictions on the interactions between bodies. These constraint equations, which are often very nonlinear functions of the coordinates, may then be solved to yield information regarding admissible configurations of the multi-body system. Time differentiation of the constraint equations leads to expressions which when properly manipulated lead to information concerning the velocities of points on the individual bodies and angular velocities of the bodies. Subsequent time differentation of the equations for the velocities and angular velocities leads to information concerning accelerations and angular accelerations. Recently, much attention has been focused on automating this process (see Nikravesh (1988)), thereby relegating the burdensome task of formulating and time-differentiating the constraint equations to the computer. The analyst is required to provide information regarding the initial configuration of the rigid bodies making up the system, the manner in which they are connected, and the manner in which the mechanism is driven. One drawback of kinematic analysis via formulation of constraint equations is that generalization to elastically flexible elements is non-trivial.

This paper explores the use of a direct finite element approach whereby kinematic analysis of planar multi-body systems composed of either rigid or flexible members is treated consistently. This is accomplished in a straight-forward manner by employing a finite element procedure where arbitrarily large displacements and rotations are included. A recent paper by Simo and Vu-Quoc (1986) addressing the dynamic analysis of planar multi-flexible-body systems is extended in the present paper to treat kinematic analysis of multi-rigid-body systems. The proposed formulation is also capable of handling general spatial (three dimensional) mechanisms, although examples of such are not included in this paper.

The motivation for the present work is that up until now, dynamic analysis of flexible multi-body systems has not been treated as a straight-forward extension of kinematic analysis of multi-rigid-body systems. The two procedures are often approached in a completely inconsistent manner. This is not necessary, as this paper will show. Two of the often cited papers are by Song and Haug (1980) and Sunada and Dubowsky (1981). The formulations in these papers do not permit reduction to kinematic analysis of multi-rigid-body mechanisms, only dynamic analyses are discussed. This is not meant to be a criticism, only a recognition of a limitation that can be overcome rather straightforwardly.

The finite element method described herein requires definition of the initial configuration of the multi-body system with the standard specification of element connectivity and nodal coordinates. The nodes are conveniently located at the joints connecting the individual links. Presently, the formulation can

handle revolute joints (e.g. hinges) and translational joints (e.g. sliders). The finite element equilibrium equations are nonlinear functions of the nodal displacement (and rotation) quantities. To determine subsequent configurations of the system as it is driven by certain specified nodal displacements and/or rotations, a nonlinear system of equations must be solved repeatedly. A Newton-Raphson iterative process is used for this this task. The associated tangent stiffness matrix (or Jacobian matrix) is symmetric and banded, as is typical for finite elements. A symmetric Jacobian matrix is not present in the traditional constraint equation approach described above. During Newton-Raphson iteration, the individual elements are allowed to deform elastically, but when convergence is obtained, the elements are undeformed elastically, having undergone only rigid body translation and rotation. The velocities and accelerations of points on the bodies together with angular velocities and accelerations of the bodies are then obtained by solving sequentially a system of linear algebraic equations whose coefficent matrix is again the tangent stiffness matrix.

In the results section of the paper, solution of the classic four-bar linkage problem by the new finite element approach is compared with the traditional constraint equation method. Other more complex planar mechanisms are analyzed to illustrate the utility of the new method.

FORMULATION

Four-Bar Linkage- Traditional Kinematics

The essential differences between the new approach and the traditional methods of kinematic analysis are highlighted by means of a specific example, namely the often encountered four-bar linkage. Two classical means of parameterizing the configuration of the linkage, one with orientation angles, and another with Cartesian coordinates and orientation angles will be described in detail. The finite element approach will then be described and proposed as an alternative.

Orientation Angle Parameterization. The configuration of the four-bar linkage shown in Fig. 1 can be parameterized by the three time-dependent orientation angles $\theta_1(t)$, $\theta_2(t)$, $\theta_3(t)$. The lengths of the three links are denoted by l_1, l_2, and l_3, while the distance between the two support points is d. The links are connected to one another by revolute joints, or hinges. Any admissible configuration of the linkage must satisfy the following two constraint equations,

$$P_1(\theta_1,\theta_2,\theta_3) = l_1\cos\theta_1 + l_2\cos\theta_2 - l_3\cos\theta_3 - d = 0 \quad (1)$$

$$P_2(\theta_1,\theta_2,\theta_3) = l_1\sin\theta_1 + l_2\sin\theta_2 - l_3\sin\theta_3 = 0 \quad (2)$$

These two equations considered jointly may be viewed as a vector function of the three orientation angles, i.e.

$$\underline{P} = \begin{pmatrix} P_1(\theta_1,\theta_2,\theta_3) \\ P_2(\theta_1,\theta_2,\theta_3) \end{pmatrix} = \underline{0} \quad (3)$$

The (3×2) Jacobian matrix $J_{ij} = \partial P_i/\partial\theta_j$ $(i = 1,2\,;\ j = 1,2,3)$ for this problem is

$$\underline{J} = \begin{pmatrix} -l_1\sin\theta_1 & -l_2\sin\theta_2 & l_3\sin\theta_3 \\ l_1\cos\theta_1 & l_2\cos\theta_2 & -l_3\cos\theta_3 \end{pmatrix} \quad (4)$$

This matrix figures prominently in numerical computations to be discussed presently. To proceed with a kinematic analysis, one of the angles must be specified as a function of time in advance. The angle $\theta_1(t)$ has been selected for this purpose. Typically, a Newton-Raphson iterative procedure is employed to solve for the remaining two angles as a function of time. For this purpose, the following matrices are defined

$$\underline{K} = \begin{pmatrix} -l_2\sin\theta_2 & l_3\sin\theta_3 \\ l_2\cos\theta_2 & -l_3\cos\theta_3 \end{pmatrix} \quad \underline{d} = \begin{pmatrix} \theta_2 \\ \theta_3 \end{pmatrix} \quad \Delta\underline{d} = \begin{pmatrix} \Delta\theta_2 \\ \Delta\theta_3 \end{pmatrix} \quad (5)$$

Note that the matrix $\underline{K}$ is nonsymmetric.

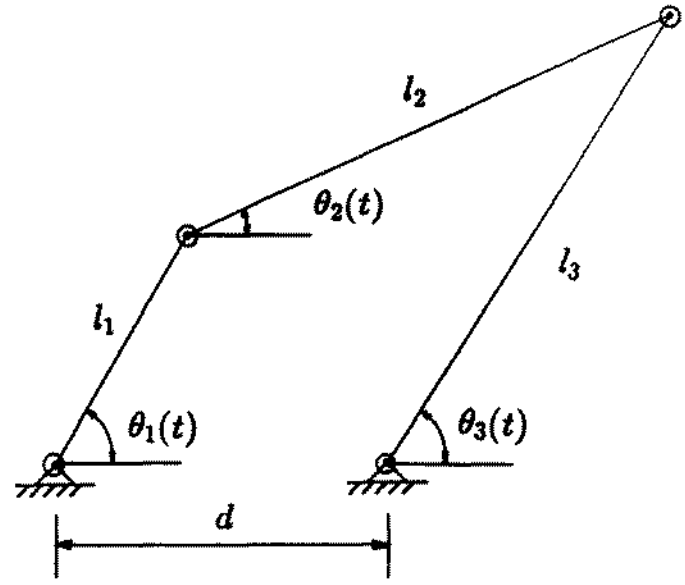

Fig. 1- Four-Bar Linkage- Orientation Angle Parameterization

The numerical scheme that advances a known configuration solution at time t_n to a new solution at time $t_{n+1} = t_n + \Delta t$ is

$n = 0$ (time step counter)

$\underline{d}_0 = \underline{d}(t_0)$, $\theta_{1,0} = \theta_1(t_0)$ (initial configuration)

$\theta_{1,n+1} = \theta_1(t_n + \Delta t)$ (value of θ_1 at t_{n+1})

$i = 0$ (nonlinear iterations counter)

$\underline{d}_{n+1}^{(i)} = \underline{d}_n$ (initial guess or predictor)

$\underline{K}^{(i)}\Delta\underline{d} = -\underline{P}^{(i)}$ (solve step)

$\underline{d}_{n+1}^{(i+1)} = \underline{d}_{n+1}^{(i)} + \Delta\underline{d}$ (corrector)

$i = i + 1$ (increment interation counter)

Convergence check:

If converged-GOTO Eq. (6k)

The iterative "loop" represented by Eqs. (6f)-(6j) is repeated until some acceptable measure of convergence is achieved. Very often, convergence is based on reduction of the Euclidean norm of $\underline{P}^{(i)}$ to a certain fraction of its initial value $\underline{P}^{(0)}$ With this algorithm, the vector $\underline{d}$ can be computed as a function of time.

The angular velocities are then determined by taking the time derivative of the constraint equations and expressing the result in matrix notation, i.e.

$$\underline{\dot{P}} = \frac{\partial \underline{P}}{\partial t} = \begin{pmatrix} -l_1 \sin\theta_1 & -l_2 \sin\theta_2 & l_3 \sin\theta_3 \\ l_1 \cos\theta_1 & l_2 \cos\theta_2 & -l_3 \cos\theta_3 \end{pmatrix} \begin{pmatrix} \dot{\theta}_1 \\ \dot{\theta}_2 \\ \dot{\theta}_3 \end{pmatrix} = \underline{0} \tag{7}$$

Since $\dot{\theta}_1(t)$ is specified in this example, this matrix equation can be partitioned to produce a system of linear algebraic equations that determine the unknown angular velocities $\dot{\theta}_2$, $\dot{\theta}_3$,

$$\begin{pmatrix} -l_2 \sin\theta_2 & l_3 \sin\theta_3 \\ l_2 \cos\theta_2 & -l_3 \cos\theta_3 \end{pmatrix} \begin{pmatrix} \dot{\theta}_2 \\ \dot{\theta}_3 \end{pmatrix} = \begin{pmatrix} l_1\dot{\theta}_1 \sin\theta_1 \\ -l_1\dot{\theta}_1 \cos\theta_1 \end{pmatrix} \tag{8}$$

This equation may be written in matrix form as

$$\underline{K}\underline{\dot{d}} = \underline{P}_v \tag{9}$$

where

$$\underline{\dot{d}} = \begin{pmatrix} \dot{\theta}_2 \\ \dot{\theta}_3 \end{pmatrix} \qquad \underline{P}_v = \begin{pmatrix} l_1\dot{\theta}_1 \sin\theta_1 \\ -l_1\dot{\theta}_1 \cos\theta_1 \end{pmatrix} \tag{10}$$

Of course, solving for $\dot{\theta}_2(t)$, $\dot{\theta}_3(t)$ cannot be accomplished until the configuration of the system has been determined by solving the nonlinear constraint equations, given by Eqs. (1)-(2), for $\theta_2(t)$, $\theta_3(t)$.

The angular accelerations are then obtained by taking the time derivative of the velocity equations, i.e. Eq. (7). After partitioning the resulting matrix equation, a system of linear algebraic equations that determine the unknown angular accelerations $\ddot{\theta}_2$, $\ddot{\theta}_3$ emerges,

$$\underline{K}\underline{\ddot{d}} = \underline{P}_a \tag{11}$$

where

$$\underline{\ddot{d}} = \begin{pmatrix} \ddot{\theta}_2 \\ \ddot{\theta}_3 \end{pmatrix}$$

$$\underline{P}_a = \begin{pmatrix} l_1\dot{\theta}_1^2 \cos\theta_1 + l_2\dot{\theta}_2^2 \cos\theta_2 - l_3\dot{\theta}_3^2 \cos\theta_3 + l_1\ddot{\theta}_1 \sin\theta_1 \\ l_1\dot{\theta}_1^2 \sin\theta_1 + l_2\dot{\theta}_2^2 \sin\theta_2 - l_3\dot{\theta}_3^2 \sin\theta_3 - l_1\ddot{\theta}_1 \cos\theta_1 \end{pmatrix} \tag{12}$$

Thus, the process of computing the configuration, angular velocities, and angular accelerations takes place sequentially.

Attention will now be focused on another way of parameterizing the four-bar linkage system.

Cartesian Coordinate Parameterization. The configuration of the four-bar linkage shown in Fig. 2 can be parameterized in terms of the Cartesian coordinates of the mass center of each link, together with the angle that each link makes with horizontal. For the present example, the links will be treated as homogeneous and prismatic, and thus the mass center will be

$$P_1(x_1, y_1, \ldots, \theta_3) = x_1 - \frac{l_1}{2}\cos\theta_1 = 0 \tag{13}$$

$$P_2(x_1, y_1, \ldots, \theta_3) = y_1 - \frac{l_1}{2}\sin\theta_1 = 0 \tag{14}$$

$$P_3(x_1, y_1, \ldots, \theta_3) = x_1 + \frac{l_1}{2}\cos\theta_1 - (x_2 - \frac{l_2}{2}\cos\theta_2) = 0 \tag{15}$$

$$P_4(x_1, y_1, \ldots, \theta_3) = y_1 + \frac{l_1}{2}\sin\theta_1 - (y_2 - \frac{l_2}{2}\sin\theta_2) = 0 \tag{16}$$

$$P_5(x_1, y_1, \ldots, \theta_3) = x_2 + \frac{l_2}{2}\cos\theta_2 - (x_3 + \frac{l_3}{2}\cos\theta_3) = 0 \tag{17}$$

$$P_6(x_1, y_1, \ldots, \theta_3) = y_2 + \frac{l_2}{2}\sin\theta_2 - (y_3 + \frac{l_3}{2}\sin\theta_3) = 0 \tag{18}$$

$$P_7(x_1, y_1, \ldots, \theta_3) = x_3 - \frac{l_3}{2}\cos\theta_3 - d = 0 \tag{19}$$

$$P_8(x_1, y_1, \ldots, \theta_3) = y_3 - \frac{l_3}{2}\sin\theta_3 = 0 \tag{20}$$

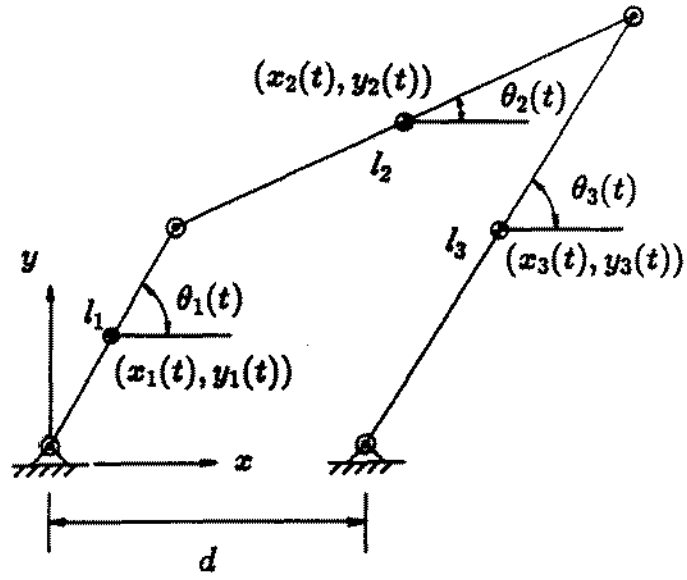

Fig. 2- Four-Bar Linkage- Cartesian Coordinate Parameterization

The corresponding (8×9) Jacobian matrix for this problem is

$$\underline{J} = \begin{pmatrix} 1 & 0 & \frac{l_1}{2}\sin\theta_1 & 0 & 0 & 0 & 0 & 0 & 0 \\ 0 & 1 & -\frac{l_1}{2}\cos\theta_1 & 0 & 0 & 0 & 0 & 0 & 0 \\ 1 & 0 & -\frac{l_1}{2}l_1\sin\theta_1 & -1 & 0 & -\frac{l_2}{2}\sin\theta_2 & 0 & 0 & 0 \\ 0 & 1 & \frac{l_1}{2}\cos\theta_1 & 0 & -1 & \frac{l_2}{2}\cos\theta_2 & 0 & 0 & 0 \\ 0 & 0 & 0 & 1 & 0 & -\frac{l_2}{2}\sin\theta_2 & -1 & 0 & \frac{l_3}{2}\sin\theta_3 \\ 0 & 0 & 0 & 0 & 1 & \frac{l_2}{2}\cos\theta_2 & 0 & -1 & -\frac{l_3}{2}\cos\theta_3 \\ 0 & 0 & 0 & 0 & 0 & 0 & 1 & 0 & \frac{l_3}{2}\sin\theta_3 \\ 0 & 0 & 0 & 0 & 0 & 0 & 0 & 1 & -\frac{l_3}{2}\cos\theta_3 \end{pmatrix} \tag{21}$$

As in the angular coordinate parameterization, the angle $\theta_1(t)$ will be regarded as specified in advance. Again, the Newton-Raphson iterative procedure outlined above is readily employed to solve for the remaining eight coordinates as a function of time.

For this purpose, the following matrices are defined

$$\underline{K} = \begin{pmatrix} 1 & 0 & 0 & 0 & 0 & 0 & 0 & 0 \\ 0 & 1 & 0 & 0 & 0 & 0 & 0 & 0 \\ 1 & 0 & -1 & 0 & -\frac{l_2}{2}\sin\theta_2 & 0 & 0 & 0 \\ 0 & 1 & 0 & -1 & \frac{l_2}{2}\cos\theta_2 & 0 & 0 & 0 \\ 0 & 0 & 1 & 0 & -\frac{l_2}{2}\sin\theta_2 & -1 & 0 & \frac{l_3}{2}\sin\theta_3 \\ 0 & 0 & 0 & 1 & \frac{l_2}{2}\cos\theta_2 & 0 & -1 & -\frac{l_3}{2}\cos\theta_3 \\ 0 & 0 & 0 & 0 & 0 & 1 & 0 & \frac{l_3}{2}\sin\theta_3 \\ 0 & 0 & 0 & 0 & 0 & 0 & 1 & -\frac{l_3}{2}\cos\theta_3 \end{pmatrix}$$

$$\underline{d} = \begin{pmatrix} x_1 \\ y_1 \\ x_2 \\ y_2 \\ \theta_2 \\ x_3 \\ y_3 \\ \theta_3 \end{pmatrix} \qquad \Delta\underline{d} = \begin{pmatrix} \Delta x_1 \\ \Delta y_1 \\ \Delta x_2 \\ \Delta y_2 \\ \Delta\theta_2 \\ \Delta x_3 \\ \Delta y_3 \\ \Delta\theta_3 \end{pmatrix} \tag{22}$$

Once again, the matrix $\underline{K}$ is nonsymmetric.

The velocities and angular velocities are determined by taking the time derivative of the constraint equations. The resulting matrix equation is partitioned to enable solution for the unknown velocities and angular velocities $\dot{x}_1$, $\dot{y}_1$, $\dot{x}_2$, $\dot{y}_2$, $\dot{\theta}_2$, $\dot{x}_3$, $\dot{y}_3$, $\dot{\theta}_3$. The matrix equation that determines these quantities is

$$\underline{K}\dot{\underline{d}} = \underline{P}_v \tag{23}$$

where

$$\dot{\underline{d}} = \begin{pmatrix} \dot{x}_1 \\ \dot{y}_1 \\ \dot{x}_2 \\ \dot{y}_2 \\ \dot{\theta}_2 \\ \dot{x}_3 \\ \dot{y}_3 \\ \dot{\theta}_3 \end{pmatrix} \qquad \underline{P}_v = \begin{pmatrix} -\frac{l_1}{2}\dot{\theta}_1\sin\theta_1 \\ \frac{l_1}{2}\dot{\theta}_1\cos\theta_1 \\ \frac{l_1}{2}\dot{\theta}_1\sin\theta_1 \\ -\frac{l_1}{2}\dot{\theta}_1\cos\theta_1 \\ 0 \\ 0 \\ 0 \\ 0 \end{pmatrix} \tag{24}$$

The velocities and angular velocities are determined by solving the linear system of algebraic equations represented by Eq. (23).

The accelerations and angular accelerations are then obtained by taking the time derivative of the velocity equations, i.e. Eq. (23). After partitioning the resulting matrix as above, a matrix equation that determines the unknown accelerations and angular accelerations emerges

$$\underline{K}\ddot{\underline{d}} = \underline{P}_a \tag{25}$$

where

$$\ddot{\underline{d}} = \begin{pmatrix} \ddot{x}_1 \\ \ddot{y}_1 \\ \ddot{x}_2 \\ \ddot{y}_2 \\ \ddot{\theta}_2 \\ \ddot{x}_3 \\ \ddot{y}_3 \\ \ddot{\theta}_3 \end{pmatrix} \qquad \underline{P}_a = \begin{pmatrix} -\frac{l_1}{2}\dot{\theta}_1^2\cos\theta_1 \\ -\frac{l_1}{2}\dot{\theta}_1^2\sin\theta_1 \\ \frac{l_1}{2}\dot{\theta}_1^2\cos\theta_1 + \frac{l_2}{2}\dot{\theta}_2^2\cos\theta_2 \\ \frac{l_1}{2}\dot{\theta}_1^2\sin\theta_1 + \frac{l_2}{2}\dot{\theta}_2^2\sin\theta_2 \\ \frac{l_2}{2}\dot{\theta}_2^2\cos\theta_2 - \frac{l_3}{2}\dot{\theta}_3^2\cos\theta_3 \\ \frac{l_2}{2}\dot{\theta}_2^2\sin\theta_2 - \frac{l_3}{2}\dot{\theta}_3^2\sin\theta_3 \end{pmatrix} \tag{26}$$

A numerical study exhibiting the relative merits of the parameterizations discussed above will be presented later in the paper.

Flexible Finite Element Parameterization

A radically different way to solve the same problem described above is to regard the links as elastically flexible. In the procedure to be described shortly, a nonlinear vector equation governs admissible configurations just as described above. During the associated iterative solution procedure to establish such configurations, the individual links are allowed to undergo axial, bending, and shearing deformations. Corresponding axial forces, shear forces, and bending moments naturally arise when elastic deformations are considered. It is the equlilibrium of these internal forces and moments that governs the configuration of a multi-body system, be it rigid or elastically flexible. If a certain "deformable" multi-body system has an admissible configuration where the elastic deformations happen to vanish, the proposed numerical algorithm will seek it out. This method of analysis is new and represents a departure from the traditional method of forming constraint equations based solely on geometrical considerations and then time differentiating to obtain velocities and accelerations. The prime motivation for adopting this approach is to provide a method that is consistent with dynamic analysis of flexible multi-body systems.

The new method described in this paper is an extension of a recent paper dealing with the dynamics of elastically flexible beams undergoing large overall motions by Simo and Vu-Quoc (1986). The present work extends the methodology described in their work to kinematic analysis of multi-rigid-body systems. The resulting computational scheme is completely consistent with standard notions of finite element spatial discretization of a structure, and is amenable to coding following standard finite element data processing procedures. For the linkage systems described earlier, one finite element is required per link, and nodes are located at the revolute joints. The formulation relies crucially on development of a finite element capable of accomodating simultaneous large overall rigid body motions and elastic deformations. A brief summary of the governing partial differential equations (PDE's) and associated finite element matrices will be presented to render the present paper complete. A large deformation beam element serves as a basic building block for the new method. Individual elements can then be assembled following standard procedures. The following discussion assumes the reader is generally familiar with finite element principles.

The basic kinematic assumptions proposed by Simo and Vu-Quoc (1986) for the large deformation beam theory are shown in Fig. 3. Inertially fixed unit vectors $\underline{e}_1$ and $\underline{e}_2$ are shown. The undeformed elastic axis of the beam is parallel to $\underline{e}_1$. For

trarily large translations and rotations. Cross sections do not necessarily remain perpendicular to the elastic axis, thus admitting transverse shear strains. The symbols $u_1(X)$ and $u_2(X)$ denote the two translational components of the motion of the cross section centroid, while $\theta(X)$ indicates the rotation of the cross section. The axial, shear, and bending strains: Γ_1, Γ_2, κ, respectively, associated with this motion and presented in matrix notation are

$$\begin{pmatrix} \Gamma_1 \\ \Gamma_2 \\ \kappa \end{pmatrix} = \underline{\Lambda}^T \begin{pmatrix} 1 + u_1' - \cos\theta \\ u_2' - \sin\theta \\ \theta' \end{pmatrix} \tag{27}$$

where

$$\underline{\Lambda} = \begin{pmatrix} \cos\theta & -\sin\theta & 0 \\ \sin\theta & \cos\theta & 0 \\ 0 & 0 & 1 \end{pmatrix} \tag{28}$$

The superposed ^{T} indicates a matrix transpose operation and the superposed prime $'$ indicates differentation with respect to X. Clearly, u_1, u_2, and θ are functions of X.

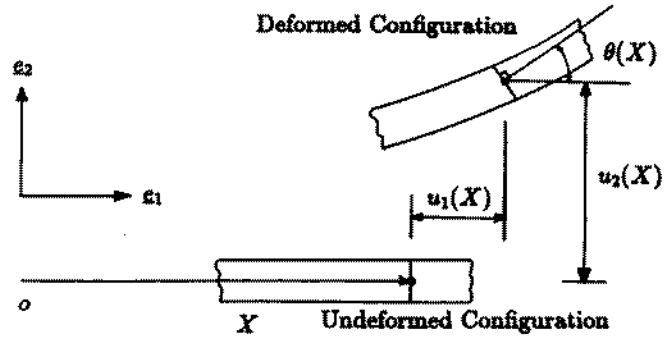

Fig. 3- Kinematics- Large Deformation Beam Theory

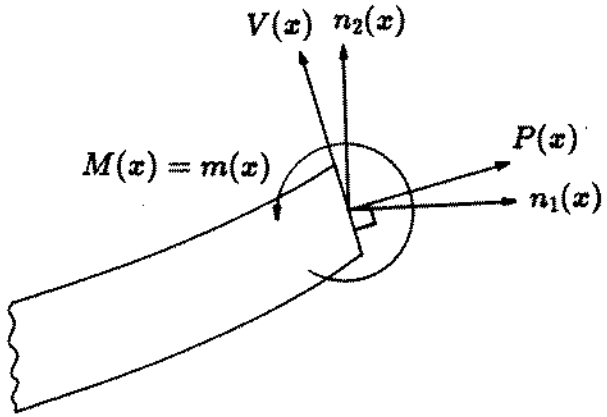

Fig. 4- Cross Section Force and Moment

The relevant cross section force and moment quantities are shown in Fig. 4. The forces may be referred to either the inertially fixed directions specified by $\underline{e}_1$, $\underline{e}_2$ through the quantities $n_1(X)$ and $n_2(X)$. Alternatively, forces may be referred to directions tangent and normal to the deformed cross section, $P(X)$ and $V(X)$. Similarly, the moment on the cross section is indicated by either of two symbols, $m(X)$ or $M(X)$, where $m(X) = M(X)$. The cross section force and moment systems are related via the rotation matrix $\underline{\Lambda}$,

$$\begin{pmatrix} n_1 \\ n_2 \\ m \end{pmatrix} = \underline{\Lambda} \begin{pmatrix} P \\ V \\ M \end{pmatrix} \tag{29}$$

For a linear elastic material, appropriate constitutive equations are

$$\begin{pmatrix} P \\ V \\ M \end{pmatrix} = \underline{C} \begin{pmatrix} \Gamma_1 \\ \Gamma_2 \\ \kappa \end{pmatrix} \quad \text{where} \quad \underline{C} = \begin{pmatrix} EA & 0 & 0 \\ 0 & kGA & 0 \\ 0 & 0 & EI \end{pmatrix} \tag{30}$$

where A and I are the cross sectional area and second moment of area, E and G are the modulus of elasticity and shear modulus, and k is the shear area ratio ($k = 5/6$ for a rectangular cross section). Defining a new vector $\underline{n}$, it is also apparent that

$$\underline{n} = \begin{pmatrix} n_1 \\ n_2 \\ m \end{pmatrix} = \underline{\Lambda C \Lambda}^T \begin{pmatrix} 1 + u_1' - \cos\theta \\ u_2' - \sin\theta \\ \theta' \end{pmatrix} \tag{31}$$

The PDE's governing the large deformation beam theory are derived by considering static force and moment equilibrium of a deformed differential element of the beam as shown in Fig. 5. The result of this calculation is

$$\left(\tilde{\underline{\Lambda}} \tilde{\underline{C}} \tilde{\underline{\Lambda}}^T \begin{pmatrix} 1 + u_1' - \cos\theta \\ u_2' - \sin\theta \end{pmatrix} \right)' = \underline{0} \tag{32}$$

$$EI\theta'' + \begin{pmatrix} -u_2' \\ 1 + u_1' \end{pmatrix} \tilde{\underline{\Lambda}} \tilde{\underline{C}} \tilde{\underline{\Lambda}}^T \begin{pmatrix} 1 + u_1' - \cos\theta \\ u_2' - \sin\theta \end{pmatrix} = 0 \tag{33}$$

where

$$\tilde{\underline{\Lambda}} = \begin{pmatrix} \cos\theta & -\sin\theta \\ \sin\theta & \cos\theta \end{pmatrix} \qquad \tilde{\underline{C}} = \begin{pmatrix} EA & 0 \\ 0 & kGA \end{pmatrix} \tag{34}$$

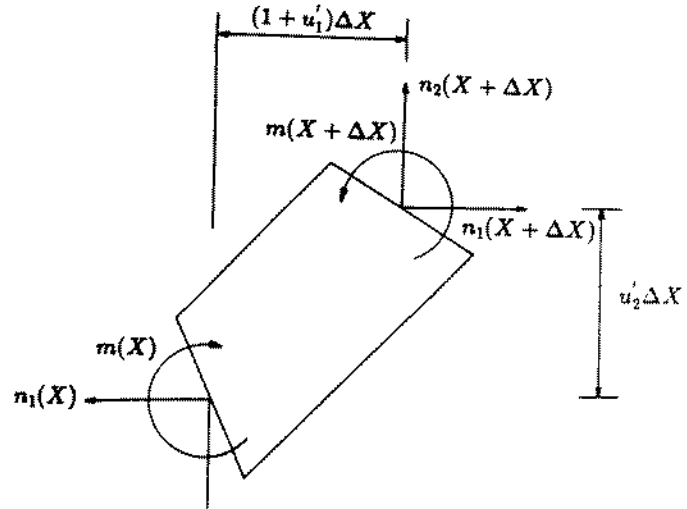

These equations are valid assuming distributed forces do not act on the beam. Simo and Vu-Quoc arrived at this same result by applying variational principles. Since Eq. (32) is a vector equation, it yields two PDE's when expanded. Thus, these two equations considered together with Eq. (33) are the three PDE's governing the large deformation beam theory.

Simo and Vu-Quoc have discussed in detail the finite element discretization of the PDE's represented by Eqs. (32)-(33). The numerical results presented in the present paper are based on an implementation using a two-node finite element employing linear shape functions. A typical element and its associated nodal degrees of freedom is shown in Fig. 6. The discretized PDE's result in a finite element equation (element level) of the form,

$$\underline{p}^e(\underline{d}^e) = \underline{f}^e_{ext} \tag{35}$$

where

$$\underline{d}^e = (\, d^e_1 \quad d^e_2 \quad d^e_3 \quad d^e_4 \quad d^e_5 \quad d^e_6 \,)^T \tag{36}$$

is the element displacement vector. The symbol $\underline{p}^e(\underline{d}^e)$ denotes the so-called element "internal force vector" that depends nonlinearly on the nodal displacements/rotations stored in vector $\underline{d}^e$. The element external force vector is denoted by $\underline{f}^e_{ext}$, and contains contributions from forces and/or moments acting at the two nodal points.

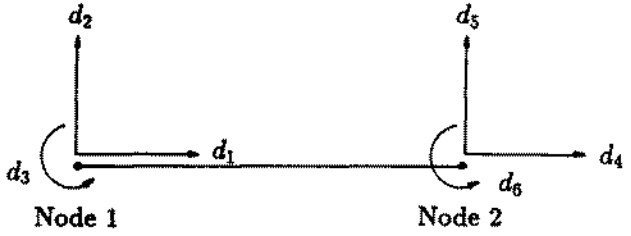

Fig. 6- Two Node Beam Element- Nodal Degree of Freedom Numbering

Kinematic analysis is independent of the forces which may act on a mechanical system. In fact, any such forces that do act on the actual system may be considered absent during kinematic analysis. Thus, for the large deformation finite element, the following equation must be satisfied during a kinematic analysis.

$$\underline{p}^e(\underline{d}^e) = \underline{0} \tag{37}$$

This equation may be viewed as a constraint equation on the finite element nodal displacements. The internal force vector (6×1) is formed computationally by evaluating the following integral over a typical finite element whose nodal points are located at X^e_1 and X^e_2 in the initial configuration.

$$\underline{p}^e = \int_{X^e_1}^{X^e_2} (\underline{D}_1\underline{\Psi})^T \underline{n} dX \tag{38}$$

where

$$\underline{\Psi} = \begin{pmatrix} N_1(X) & 0 & 0 & N_2(X) & 0 & 0 \\ 0 & N_1(X) & 0 & 0 & N_2(X) & 0 \\ 0 & 0 & N_1(X) & 0 & 0 & N_2(X) \end{pmatrix} \tag{40}$$

The linear finite element shape functions are denoted by $N_1(X)$ and $N_2(X)$, and are defined explicitly by

$$N_1(x) = -\frac{X - X^e_2}{X^e_2 - X^e_1} \qquad N_2(X) = \frac{X - X^e_1}{X^e_2 - X^e_1} \tag{41}$$

In practice, the integral in Eq. (38) would be evaluated by Gauss quadrature after making a change of variables so that the range of integration is $-1 \rightarrow 1$.

In order to solve the nonlinear vector function represented by Eq. (37) with the Newton-Raphson method, it is necessary to have the so-called "tangent stiffness matrix", defined by

$$\underline{k}^e = \frac{\partial \underline{p}^e}{\partial \underline{d}^e} \tag{42}$$

The tangent stiffness matrix (6×6) is formed computationally by evaluating the following integral

$$\underline{k}^e = \underline{k}^e_m + \underline{k}^e_g = \int_{X^e_1}^{X^e_2} (\underline{D}_1\underline{\Psi})^T \underline{\Lambda C \Lambda}^T (\underline{D}_1\underline{\Psi}) dX + \int_{X^e_1}^{X^e_2} (\underline{D}_2\underline{\Psi})^T \underline{G} (\underline{D}_2\underline{\Psi}) dX \tag{43}$$

where

$$\underline{D}_2 = \begin{pmatrix} d/dX & 0 & 0 \\ 0 & d/dX & 0 \\ 0 & 0 & 1 \end{pmatrix}$$

$$\underline{G} = \begin{pmatrix} 0 & 0 & -n_2 \\ 0 & 0 & n_1 \\ -n_2 & n_1 & -[(1+u_1')n_1 + u_2' n_2] \end{pmatrix} \tag{44}$$

The first integral in Eq. (43) is referred to as the material tangent stiffness $\underline{k}^e_m$, while the second integral is called the geometric tangent stiffness $\underline{k}^e_g$. The matrix $\underline{k}^e$ is symmetric.

Configuration analysis then proceeds by assembling the element internal force vectors into a global internal force vector $\underline{P}(\underline{d})$, and the element element tangent stiffness matrices into a global tangent stiffness stiffness $\underline{K}(\underline{d})$ following standard finite element data processing procedures. The global cross section displacements and rotations (hereafter simply referred to as displacements) are stored in the vector $\underline{d}$. These quantities are then used in the Newton-Raphson iterative procedure described earlier. After the iterative procedure converges on an admissible configuration, the geometric tangent stiffness is zero because the cross sectional forces and moment n_1, n_2, and m must vanish in a kinematic analysis. However, the geometric stiffness is non-zero during the iterative solution procedure, and cannot be neglected. However, as will be seen presently, the tangent stiffness also enters the velocity and acceleration analyses. For these calculations, only the material part of the tangent stiffness must

The partial derivative of the internal force with respect to the nodal displacements has already been defined as the tangent stiffness. For an elastically undeformed structure, $\underline{k}^e = \underline{k}^e_m$, and so the velocity equations are

$$\underline{k}^e_m \dot{\underline{d}}^e = \underline{0} \tag{46}$$

After partitioning this equation to account for any specified nodal velocities and/or angular velocities, and assembling the resulting equations into global matrices and vectors, the following matrix equation will emerge

$$\underline{K}\dot{\underline{d}} = \underline{P}_v \tag{47}$$

The vector $\underline{P}_v$ contains information regarding the specified nodal velocities and/or angular velocities. The unknown velocities and angular velocities are determined by solving the linear system of algebraic equations represented by Eq. (47). The task is greatly simplified because the coefficient matrix $\underline{K}$ is symmetric!

Acceleration and angular acceleration analysis follows the velocity analysis by noting that

$$\frac{\partial}{\partial t}\left(\frac{\partial \underline{p}^e}{\partial t}\right) = \left(\frac{\partial \underline{p}^e}{\partial \underline{d}^e}\right)\ddot{\underline{d}}^e + \frac{\partial}{\partial t}\left(\frac{\partial \underline{p}^e}{\partial \underline{d}^e}\right)\dot{\underline{d}}^e = \underline{0} \tag{48}$$

or

$$\underline{k}^e_m \ddot{\underline{d}}^e = -\left(\frac{\partial \underline{k}^e_m}{\partial \underline{d}^e}\dot{\underline{d}}^e\right)\dot{\underline{d}}^e \tag{49}$$

Again, the fact that $\underline{k}^e = \underline{k}^e_m$ for an elastically undeformed structure has been used. In order to explicitly define the components of the right hand side of Eq. (49), it is useful to rewrite the matrix expression as

$$\underline{k}^e_m \ddot{\underline{d}}^e = -\left(\sum_{i=1}^{6} \frac{\partial \underline{k}^e_m}{\partial d^e_i}\dot{d}^e_i\right)\dot{\underline{d}}^e \tag{50}$$

The derivative of the material tangent stiffness matrix with respect to the nodal displacements is

$$\frac{\partial \underline{k}^e_m}{\partial d^e_i} = \int_{X^e_1}^{X^e_2} (\underline{D}_{1,i}\underline{\Psi})^T \underline{\Lambda C \Lambda}^T (\underline{D}_1\underline{\Psi}) dX + \int_{X^e_1}^{X^e_2} (\underline{D}_1\underline{\Psi})^T \underline{\Lambda C \Lambda}^T (\underline{D}_{1,i}\underline{\Psi}) dX$$
$$+ \int_{X^e_1}^{X^e_2} (\underline{D}_1\underline{\Psi})^T (\underline{\Lambda}_{,i}\underline{C}\underline{\Lambda}^T + \underline{\Lambda C \Lambda}^T_{,i})(\underline{D}_1\underline{\Psi}) dX \tag{51}$$

where

$$\underline{D}_{1,i} = \begin{pmatrix} 0 & 0 & \delta_{2i}N'_1 + \delta_{5i}N'_2 \\ 0 & 0 & -(\delta_{1i}N'_1 + \delta_{4i}N'_2) \\ 0 & 0 & 0 \end{pmatrix} \tag{52}$$

$$\underline{\Lambda}_{,i} = (\delta_{3i}N_1 + \delta_{6i}N_2)\begin{pmatrix} -\sin\theta & -\cos\theta & 0 \\ \cos\theta & -\sin\theta & 0 \\ 0 & 0 & 0 \end{pmatrix} \tag{53}$$

The symbol δ_{ij}, $i,j = 1,2,\ldots,6$ indicates the Kronecker delta. The notation $()_{,i}$ indicates partial differentiation with respect to

$$\underline{K}\ddot{\underline{d}} = \underline{P}_a \tag{54}$$

An important note regarding implementation that was omitted by Simo and Vu-Quoc should be made at this time. The matrices and vectors defined above are valid provided that the beam element is parallel to $\underline{e}_1$ (horizontal) in the initial configuration. Should the element be initially inclined with respect to the horizontal, a coordinate transformation must be effected. The details of such are included in standard texts on finite elements (e.g. Cook (1981)). In this case, before configuration analysis, the element displacement vector, internal force vector, and tangent stiffness matrix must be "rotated" by appropriate pre and post multiplication by an orthogonal matrix. For the subsequent velocity and acceleration analyses, the velocity vector, $\underline{P}_v$ vector, acceleration vector, and $\underline{P}_a$ vector must also be rotated.

A second implementation issue worth mentioning is the incorporation of hinges or revolute joints. This is handled very simply with the concept of "double-noding." When two or more elements are connected at a common hinge point, each adjoining element is assigned its own node at the hinge point. These nodal points are assigned the same coordinates in the initial configuration. Translational degrees of freedom at these two nodal point must be coupled, while the rotational degrees of freedom are independent. This feature is easily accounted for during the element assembly process.

Sliding Joints- Contact Algorithm. The presence of a prismatic or "sliding" joint within a multi-body system may be handled very conveniently by extending a contact algorithm presented by Simo, et. al. (1985). Fig. 7 shows a typical sliding joint within a multi-body mechanism. In our formulation, a prismatic joint is idealized by constraining a nodal point of one element to slide along another element. The sliding node is termed the "slave" node, while the element it makes contact with is called the "master" element. The nodes associated with the master element are termed the master nodes. A penalty procedure is used to enforce, in an approximate manner, the condition that the slave node remain in contact with the master element. However, during the nonlinear iterations associated with the configuration analysis, the slave node is generally not in contact with the master element, thus violating the constraint. The penalty procedure employed here has a very clear physical interpretation. The sliding joint constraint may be enforced by placing a hypothetical linear spring between the slave node and the master element.

A description of the kinematics and contact forces for a typical slave node and master nodes (numbered 1 and 2) is presented in Fig. 8. The position vectors of these three node points (with respect to an origin at point O) are indicated by $\underline{P}_s$, $\underline{P}_1$, and $\underline{P}_2$, respectively. Components of these vectors are expressed in terms of the unit vectors $\underline{e}_1$ and $\underline{e}_2$. The measure numbers of these vectors are conveniently represented as follows,

$$\underline{P}_s = (p^s_1\ p^s_2)^T \quad \underline{P}_1 = (p^1_1\ p^1_2)^T \quad \underline{P}_2 = (p^2_1\ p^2_2)^T \tag{55}$$

The length s_l of the master element is determined by the [illegible]a

where β is the angle between $\underline{e}_1$ and $\underline{t}$. The unit vector normal to the master element is

$$\underline{n}_r = (-\sin\beta \;\; \cos\beta)^T \tag{58}$$

During the iterative process to determine configurations, the slave node does not necessarily lie along the line joining nodes 1 and 2. The "gap" (see Fig. 8) between the slave node and master element is calculated with the formula

$$g = (\underline{P}_s - \underline{P}_1) \cdot \underline{n}_r \tag{59}$$

The position of the slave node with respect to the master nodes is parameterized with a dimensionless coordinate α as follows

$$\alpha = \frac{(\underline{P}_s - \underline{P}_1) \cdot \underline{t}}{s_l} \tag{60}$$

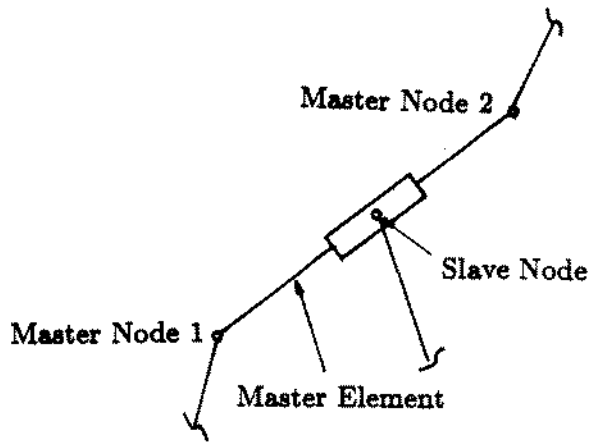

Fig. 7- Schematic of a Sliding Joint Showing Slave and Master Elements

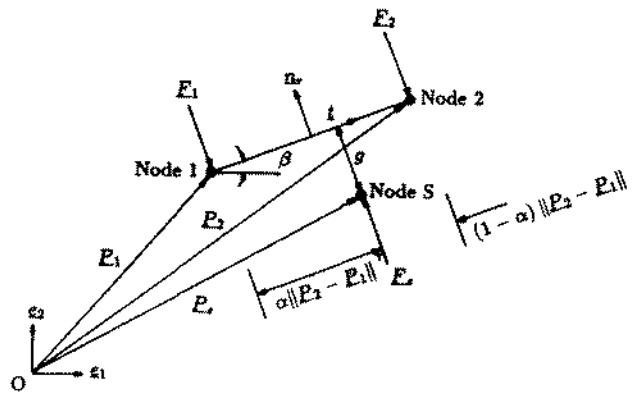

Fig. 8- Kinematics and Forces- Sliding Joint

Three vectors (6 by 1), $\underline{N}_s$,$\underline{N}_m$ and $\underline{T}_s$, that play a prominent role in the subsequent contact algorithm are

$$\underline{N}_s = (-\sin\beta, \cos\beta, (1-\alpha)\sin\beta, -(1-\alpha)\cos\beta, \alpha\sin\beta, -\alpha\cos\beta)^T \tag{61}$$

$$\underline{N}_m = (0, 0, \sin\beta, -\cos\beta, -\sin\beta, \cos\beta)^T \tag{62}$$

$$\underline{T}_s = (\cos\beta, \sin\beta, -(1-\alpha)\cos\beta, -(1-\alpha)\sin\beta, -\alpha\cos\beta, -\alpha\sin\beta)^T \tag{63}$$

The hypothetical spring is joined to the master element at a distance $\alpha\|\underline{P}_2 - \underline{P}_1\|$ from node 1. The spring is not active if the slave node lies on the master element. If this is not the case, the spring acts to "pull" the slave node back towards the master element to maintain the constraint. There is no moment carried across the contact point, only a concentrated force. The contact forces developed at the three nodes may be arranged in a 6 by 1 element contact force vector as follows,

$$\underline{f}^c = (\underline{F}_s, \underline{F}_1, \underline{F}_2)^T \tag{64}$$

where $\underline{F}_s$, $\underline{F}_1$, and $\underline{F}_2$ are the forces acting on nodes s, 1, and 2, respectively, due to violation of the contact constraint. Consideration of static equilibrium reveals that

$$\underline{f}^c = -k_p g \underline{N}_s \tag{65}$$

where k_p is a penalty constant that the analyst selects to control accuracy and convergence of the solution algorithm. Generally, the higher the value selected for k_p, the more accurate the satisfaction of the sliding joint constraint. However, too large a value leads to numerical ill-conditioning. Numerical experiments are necessary to determine optimum values for the penalty parameter for any given problem.

The nodal displacements associated with the contact may be represented as follows (see Fig. 9)

$$\underline{d}^s = (d_1^s \; d_2^s)^T \quad \underline{d}^1 = (d_1^1 \; d_2^1)^T \quad \underline{d}^2 = (d_1^2 \; d_2^2)^T \tag{66}$$

These six displacements associated with the contact may then be arranged in a 6 by 1 vector $\underline{d}^c$. The correspondence between the components of $\underline{d}^c$ and the components of the nodal displacements listed above is

$$\underline{d}^c = (d_1^c \; d_2^c \; d_3^c \; d_4^c \; d_5^c \; d_6^c)^T = (d_1^s \; d_2^s \; d_1^1 \; d_2^1 \; d_1^2 \; d_2^2)^T \tag{67}$$

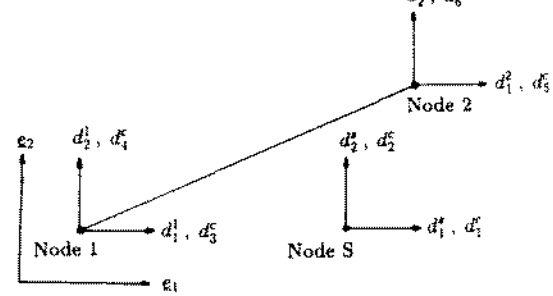

The position vectors $\underline{P}_s$, $\underline{P}_1$, and $\underline{P}_2$ may be expressed in terms of the nodal displacements as follows

$$\underline{P}_s = \underline{P}_s^0 + \underline{d}^s \tag{68}$$
$$\underline{P}_1 = \underline{P}_1^0 + \underline{d}^1 \tag{69}$$
$$\underline{P}_2 = \underline{P}_2^0 + \underline{d}^2 \tag{70}$$

where $\underline{P}_s^0$, $\underline{P}_1^0$, $\underline{P}_2^0$ are the position vectors of the three contact nodes in the undeformed (reference) configuration.

The following Jacobian (or tangent stiffness) matrix defined by

$$\underline{k}^c = \frac{\partial \underline{f}^c}{\partial \underline{d}^c} \tag{71}$$

is a vital part of the contact algorithm. A lengthy, but straighforward calculation first reported by Simo, et. al. (1985) shows that the 6 by 6 element contact tangent stiffness matrix $\underline{k}^c$ is given by

$$\underline{k}^c = -k_p \left(\underline{N}_s \underline{N}_s^T - \frac{g}{s_l} (\underline{T}_s \underline{N}_m^T + \underline{N}_m \underline{T}_s^T + \frac{g}{s_l} \underline{N}_m \underline{N}_m^T) \right) \tag{72}$$

The tangent stiffness matrix $\underline{k}^c$ can be divided into two parts,

$$\underline{k}^c = \underline{k}_s^c + \underline{k}_g^c \tag{73}$$

where

$$\underline{k}_s^c = -k_p \underline{N}_s \underline{N}_s^T \tag{74}$$

$$\underline{k}_g^c = k_p \frac{g}{s_l} (\underline{T}_s \underline{N}_m^T + \underline{N}_m \underline{T}_s^T + \frac{g}{s_l} \underline{N}_m \underline{N}_m^T) \tag{75}$$

For a multi-body system (rigid or flexible members), with sliding joints requiring consideration of contact, the global equilibrium equation is

$$\underline{P} = \underline{F}^c \tag{76}$$

where $\underline{P}$ and $\underline{F}^c$ are the global counterparts of $\underline{p}^e$ and $\underline{f}^c$. The iterative solution procedure to determine admissible configurations (and hence satisfy Eq. (76)) is modified to account for the presence of contact. The solve step in the Newton-Raphson method is now

$$(\underline{K}^{(i)} - \underline{K}^{c(i)}) \Delta \underline{d} = -\underline{P}^{(i)} + \underline{F}^{c(i)} \tag{77}$$

where $\underline{K}^{(i)}$ and $\underline{P}^{(i)}$ are the global tangent stiffness matrix and internal force vector defined earlier in the paper. The matrix $\underline{K}^{c(i)}$ is the global counterpart of the element contact tangent stiffness matrix $\underline{k}^c$.

Modification of the velocity analysis to account for the presence of contact is treated presently. The time derivative of the equilibrium equation is

$$\frac{\partial \underline{P}}{\partial \underline{d}} \dot{\underline{d}} = \frac{\partial \underline{F}^c}{\partial \underline{d}} \dot{\underline{d}} \tag{78}$$

Recall that $\dot{\underline{d}}$ is the global vector storing nodal velocities and angular velocities. Treatment of the term on the left hand side was addressed earlier. In a finite element implementation, the term $\frac{\partial \underline{F}^c}{\partial \underline{d}} \dot{\underline{d}}$ is naturally formed at the element level, i.e.

where "element" refers to a "contact element" consisting of nodes s, 1, and 2. For a converged configuration (constraints satisfied), examination of Eq. (75) reveals that $\underline{k}_g^c = 0$ because $g = 0$. Thus, only $\underline{k}_s^c$ enters the velocity analysis. After assembling the element contribution $\underline{k}_s^c \dot{\underline{d}}^c$, the matrix equation emerges,

$$(\underline{K} - \underline{K}^c) \dot{\underline{d}} = \underline{P}_v \tag{80}$$

Recall that the vector $\underline{P}_v$ contains information concerning specified velocities and angular velocities. The reader is encouraged to compare this expression with Eq. (47). Hopefully, the conclusion is that accounting for a sliding joint is quite simple.

The modifications for the acceleration analysis are somewhat more involved. Taking the time derivative of Eq. (78) gives,

$$\frac{\partial \underline{P}}{\partial \underline{d}} \ddot{\underline{d}} + \left(\frac{\partial \underline{K}}{\partial \underline{d}} \dot{\underline{d}} \right) \dot{\underline{d}} = \frac{\partial \underline{F}^c}{\partial \underline{d}} \ddot{\underline{d}} + \left(\frac{\partial \underline{K}^c}{\partial \underline{d}} \dot{\underline{d}} \right) \dot{\underline{d}} \tag{81}$$

The terms on the left-hand side of Eq. (81) were treated previously. Like in the velocity analysis, the terms involving $\underline{F}^c$ and $\underline{K}^c$ are formed at the element level, i.e.

$$\frac{\partial \underline{f}_c}{\partial \underline{d}^c} \ddot{\underline{d}}_c = \underline{k}_s^c \ddot{\underline{d}}^c \tag{82}$$

$$\left(\frac{\partial \underline{k}_s^c}{\partial \underline{d}^c} \dot{\underline{d}}^c \right) \dot{\underline{d}}^c = \left(\sum_{i=1}^{6} \frac{\partial \underline{k}_s^c}{\partial d_i^c} \dot{d}_i^c \right) \dot{\underline{d}}^c \tag{83}$$

where

$$\frac{\partial \underline{k}_s^c}{\partial d_i^c} = -k_p \left(\frac{\partial \underline{N}_s}{\partial d_i^c} \underline{N}_s^T + \underline{N}_s \frac{\partial \underline{N}_s^T}{\partial d_i^c} \right) \tag{84}$$

The various derivatives $\frac{\partial \underline{N}_s}{\partial d_i^c}$ are listed below

$$\frac{\partial \underline{N}_s}{\partial d_1^c} = \left(0, 0, \frac{-\sin\beta\cos\beta}{s_l}, \frac{\cos^2\beta}{s_l}, \frac{\sin\beta\cos\beta}{s_l}, \frac{\cos^2\beta}{s_l} \right)^T \tag{85}$$

$$\frac{\partial \underline{N}_s}{\partial d_2^c} = \left(0, 0, \frac{-\sin^2\beta}{s_l}, \frac{\sin\beta\cos\beta}{s_l}, \frac{\sin^2\beta}{s_l}, \frac{-\sin\beta\cos\beta}{s_l} \right)^T \tag{86}$$

$$\frac{\partial \underline{N}_s}{\partial d_3^c} = \left(0, -\frac{1}{s_l}, -\frac{\partial \alpha}{\partial d_3^c}\sin\beta, \right.$$
$$\left. \frac{\partial \alpha}{\partial d_3^c}\cos\beta + \frac{1-\alpha}{s_l}, \frac{\partial \alpha}{\partial d_3^c}\sin\beta, -\frac{\partial \alpha}{\partial d_3^c}\cos\beta + \frac{\alpha}{s_l} \right)^T \tag{87}$$

$$\frac{\partial \underline{N}_s}{\partial d_4^c} = \left(\frac{1}{s_l}, 0, -\frac{\partial \alpha}{\partial d_4^c}\sin\beta - \frac{1-\alpha}{s_l}, \right.$$
$$\left. \frac{\partial \alpha}{d_4^c}\cos\beta, \frac{\partial \alpha}{\partial d_4^c}\sin\beta - \frac{\alpha}{s_l}, -\frac{\partial \alpha}{\partial d_4^c}\cos\beta \right)^T \tag{88}$$

$$\frac{\partial \underline{N}_s}{\partial d_5^c} = \left(0, \frac{1}{s_l}, -\frac{\partial \alpha}{\partial d_5^c}\sin\beta, \right.$$
$$\left. \frac{\partial \alpha}{\partial d_5^c}\cos\beta - \frac{1-\alpha}{s_l}, \frac{\partial \alpha}{\partial d_5^c}\sin\beta, -\frac{\partial \alpha}{\partial d_5^c}\cos\beta - \frac{\alpha}{s_l} \right)^T \tag{89}$$

$$\frac{\partial \underline{N}_s}{\partial d_6^c} = \left(-\frac{1}{s_l}, 0, -\frac{\partial \alpha}{\partial d_6^c}\sin\beta + \frac{1-\alpha}{s_l}, \right.$$
$$\left. \frac{\partial \alpha}{\partial d_6^c}\cos\beta, \frac{\partial \alpha}{\partial d_6^c}\sin\beta + \frac{\alpha}{s_l}, -\frac{\partial \alpha}{\partial d_6^c}\cos\beta \right)^T \tag{90}$$

where

$$\frac{\partial \alpha}{\partial d_3^c} = \frac{1}{s_l}(-\cos\beta - \frac{1}{s_l}(p_1^s - p_1^1)) \tag{91}$$

$$\frac{\partial \alpha}{\partial d_4^c} = \frac{1}{s_l}\{-\sin\beta - \frac{1}{s_l}(p_2^s - p_2^1)\} \tag{92}$$

$$\frac{\partial \alpha}{\partial d_5^c} = \frac{1}{s_l^2}(p_1^2 - p_1^1) \tag{93}$$

$$\frac{\partial \alpha}{\partial d_6^c} = \frac{1}{s_l^2}(p_2^2 - p_2^1) \tag{94}$$

After the assembly procedure, the following matrix equation emerges,

$$(\underline{K} - \underline{K}^c)\underline{\tilde{d}} = \underline{P}_a \tag{95}$$

where $\underline{P}_a$ is a vector containing information regarding specified velocities, angular velocities, accelerations, and angular accelerations. As before, accelerations are determined by solving a linear system of algebraic equations that have a banded and symmetric coefficient matrix.

NUMERICAL EXAMPLES

Example 1: Four-Bar Linkage- Convergence Study

The basic four-bar mechanism was studied in order to ascertain the efficiency of the new method in comparison to the more traditional kinematic analysis methods. The orientation angle and Cartesian coordinate parameterizations were each implemented computationally and used in conjunction with the Newton-Raphson iterative procedure to predict kinematic quantities for the linkage shown in Fig. 10. The following data was used for this analysis: $l_1 = 2.0$, $l_2 = 4.0$, $l_3 = 4.0$, $E = 1.0$, $G = 1.0$, $A = 100.0$, $I = 1.0$, $k = 5/6$. It should be noted that the converged results do not depend on the values of the material properties or cross sectional properties. Convergence of the configuration analysis was considered adequate when $\|\underline{P}^{(i)}\|/\|\underline{P}^{(0)}\| < 10^{-10}$, i.e. when the Euclidean norm of $\underline{P}$ had been reduced ten orders of magnitude. Link 1 was rotated counterclockwise at an angular velocity equal to 2π rads/sec. Table 1 shows the number of iterations to convergence for the two standard methods and the finite element method (FEM) for a time step size $\Delta t = 0.025$ sec. All three methods converged in approximately the same number of iterations, typically the FEM procedure required one additional step. It is also important to consider the size and structure of the $\underline{K}$ matrix for each method, since it must be formed and factored repeatedly during Newton-Raphson iteration. For the orientation angle approach $\underline{K}$ is (2×2) and nonsymmetric, for the Cartesian coordinate method (8×8) and nonsymmetric, and for the new finite element method (9×9) and symmetric. Thus the FEM scheme involves the largest "stiffness" matrix, but it has the advantage that symmetry is present, and is hence superior to the Cartesian coordinate method as regards numerical efficiency. As pointed out by Nikravesh (1988), it is relatively difficult to develop a general purpose program based on the orientation angle parameterization. The Cartesian coordinate method is slower to converge than either of the other two methods. Table 3 shows convergence results for an extremely large time step size $\Delta t = 0.5$ sec. Here link 1 is rotated 360° in just two steps, clearly a situation where numerical difficulties would be expected. The Cartesian coordinate scheme fails to converge during the second time step in this case, while orientation angles and FEM do converge with no difficulties.

Table 1- Convergence Results for $\Delta t = 0.025$ sec.

	Number of iterations		
	Orientation Angles	Cartesian Coord.	F.E.M
t = 0.025 sec	5	5	6
t = 0.050 sec	5	5	6
t = 0.075 sec	5	5	6
t = 0.100 sec	5	5	6
t = 0.125 sec	5	4	6
t = 0.150 sec	5	4	6
t = 0.175 sec	5	4	6
t = 0.200 sec	5	4	6
t = 0.225 sec	5	4	6
t = 0.250 sec	5	4	6

Table 2- Convergence Results for $\Delta t = 0.25$ sec.

	Number of iterations		
	Orientation Angles	Cartesian Coord.	F.E.M
t = 0.25 sec	6	6	11
t = 0.50 sec	7	6	11
t = 0.75 sec	6	6	12
t = 1.00 sec	7	11	18

Table 3- Convergence Results for $\Delta t = 0.50$ sec.

	Number of iterations		
	Orientation Angles	Cartesian Coord.	F.E.M
t = 0.50 sec	8	8	11
t = 1.00 sec	9	Not Converged	13

Example 2: Four-Bar Linkage- Kinematic Analysis

Fig. 11 shows a four-bar mechanism with an additional appendage ($l_3 = 1.5$) attached to the center link. The other dimensions and physical properties were the same as the last example. For the kinematic analysis simulation using the new FEM approach, link 1 was rotated at a constant angular velocity equal to 2π rad/sec. The circles on Fig. 11 show the path of the end point of link 5 (point P) as the driving link is rotated through 360°. This result is in complete agreement with KAP- a kinematic analysis program described in the book by Nikravesh (1988). Fig. 12 shows the time history of the three orientation angles. The reader is reminded that these "orientation angles" are actually cross section rotations when viewed with respect to the finite element formulation.

Example 3: Double Parallel Crank- Redundant Mechanism

Fig. 13 shows a mechanism known as the double parallel

many kinematic analysis programs, this fact has to anticipated in advance by the analyst, or else the numerical solution scheme will fail due to a singular Jacobian matrix. This problem poses no difficulty for the FEM scheme, and no special precautions need be taken, such as removing redundant links. Fig. 13 shows the expected circular path of the hinge initially located at the upper right hand corner as the mechanism is rotated through 360°.

Example 4: Peaucellier-Lipkin Exact Straight Line Mechanism

A very interesting mechanism is shown in Fig. 14. When link 7 is rotated clockwise, point P moves down on a straight line. A simulation using the new FEM scheme verifies this behavior, as exhibited by the path (circles) shown on Fig. 14. The following data was used for this analysis: $l_1 = 3.0$, $l_2 = 1.2$, $l_3 = 1.2$, $l_4 = 1.2$, $l_5 = 1.2$, $l_6 = 3.0$, $l_7 = 1.4$, $E = 1.0$, $G = 1.0$, $A = 100.0$, $I = 1.0$, $k = 5/6$. Figs. 14a-c show the time history of the vertical component of the position, velocity, and acceleration of point P when the orientation angle of link 7 is specified as shown in the Fig. 14.

Example 5: Quick-Return Mechanism

Fig. 15 shows a quick-return mechanism that includes a sliding joint and four hinge joints. Link 1 is driven by a constant angular velocity equal to 2π rad/sec. The link lengths are $l_1 = 100$, $l_2 = 474.34$, $l_3 = 158.11$. The position, velocity, and acceleration of point P is shown in Figs. 15a-15c. Clearly, point P travels to the left a much lower velocity than it "returns" to the right.

CONCLUSIONS

A new method of kinematic analysis for certain multi-rigid-body systems employing finite element discretization has been presented. The novel feature of the method is that kinematic analysis of multi-rigid-body systems is treated in a manner completely consistent with multi-flexible-body systems. The new method is based on the fact during a kinematic analysis, any internal forces and moments may be considered zero. This is in distinct contrast to traditional kinematics approaches, whereby geometric constraint equations are solved to produce admissible configurations, and then subsequently time-differentiated to yield information concerning velocities and accelerations.

REFERENCES

Cook, R. D., 1981, *Concepts and Applications of Finite Element Analysis*, 2nd Ed., John Wiley and Sons.

Nikravesh, P. E., 1988, *Computer-Aided Analysis of Mechanical Systems*, Prentice-Hall.

Simo, J. C., et. al., 1984, "Finite Deformation Postbuckling Analysis Involving Inelasticity and Contact Constraints," *Innovative Methods for Nonlinear Problems*, Pineridge Press.

Simo, J. C., and Vu-Quoc, L., 1986, "On the Dynamics of Flexible Beams Under Large Overall Motions- The Plane Case: Parts I and II," *ASME Journal of Applied Mechanics*, Vol. 53, No. 4, pp. 849-863.

Song, J. O., and Haug, E. J., 1980, "Dynamic Analysis of Planar Flexible Mechanisms," *Computer Methods in Applied Mechanics and Engineering*, Vol. 24, pp. 359-381.

Sunada, W., and Dubowsky, S., 1981, "The Application of Finite Element Methods to the Dynamic Analysis of Flexible Spatial and Co-Planar Linkage Systems," *ASME Journal of Mechanical Design*, Vol. 103, pp. 643-651.

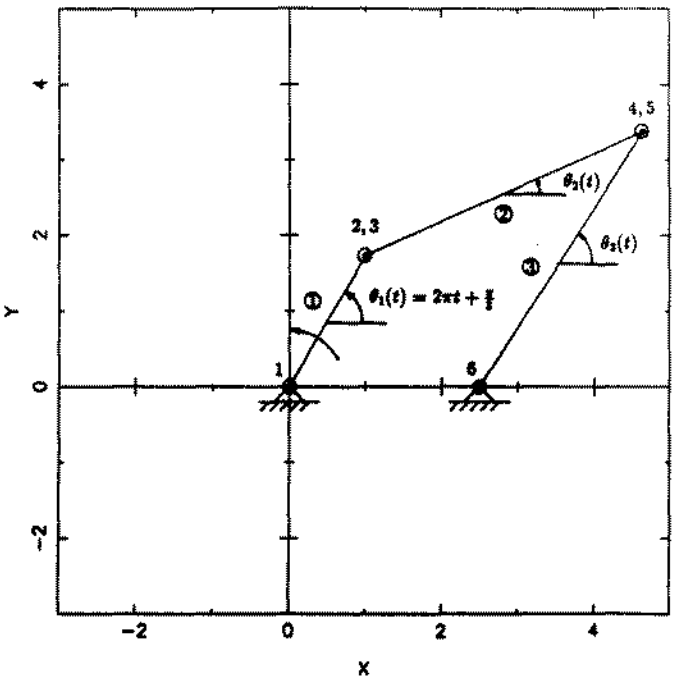

Fig. 10- Four-Bar Linkage Configuration Used For Convergence Study

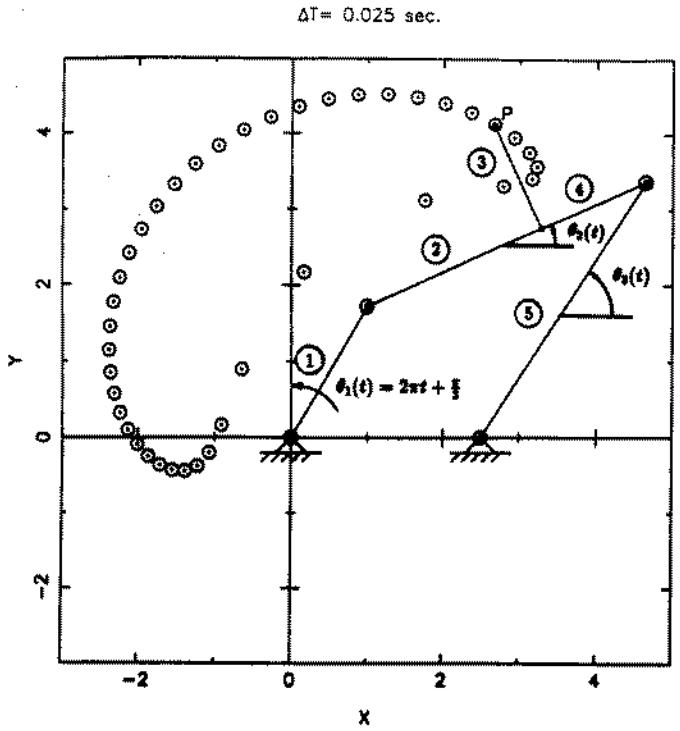

Fig. 11- Four-Bar Linkage- Motion of Appendage End Point

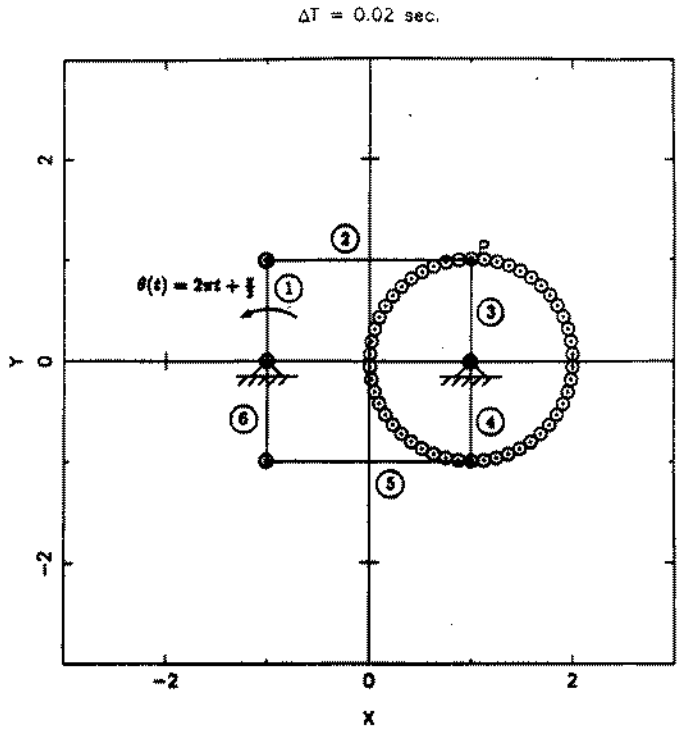

Fig. 13- Double Parallel Crank- Path of Hinge Point

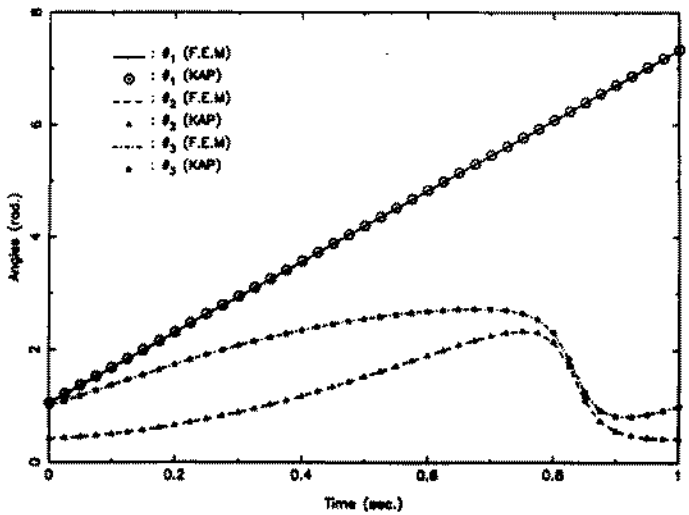

Fig. 12- Four-Bar Linkage- Time History of Orientation Angles

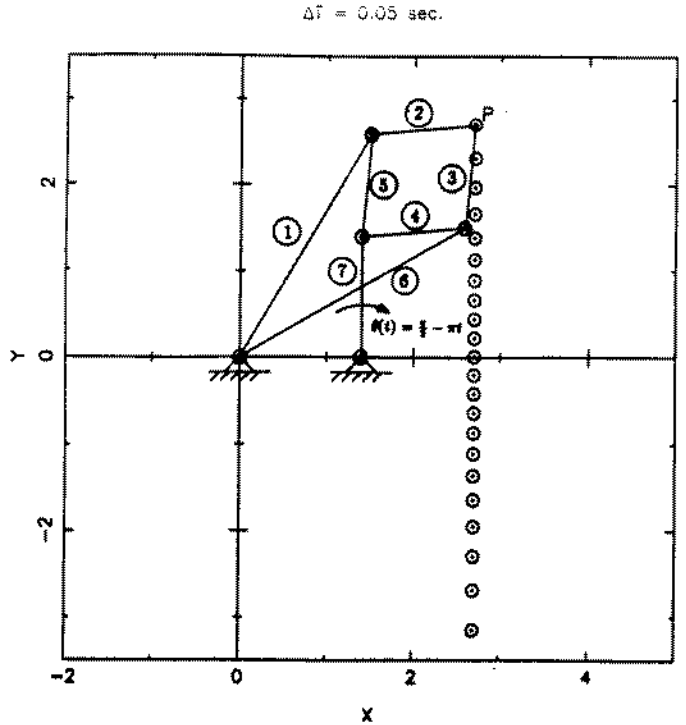

Fig. 14- Peaucellier-Lipkin Mechanism- Motion of Hinge Point P

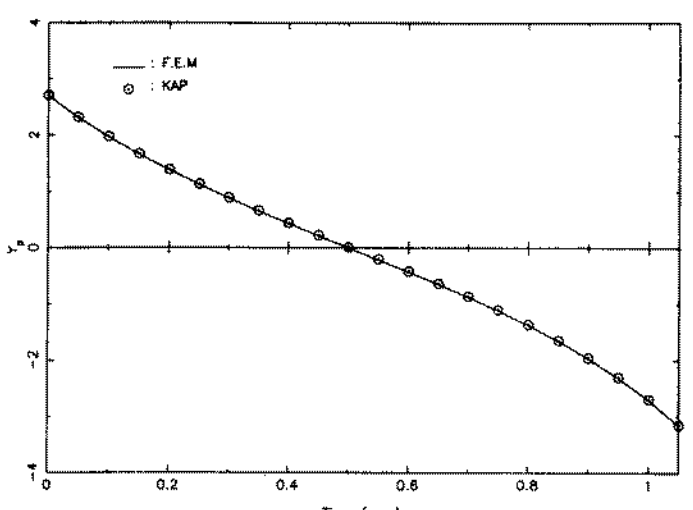

Fig. 14a- Peaucellier-Lipkin Mechanism- Time History of the Position of Point P

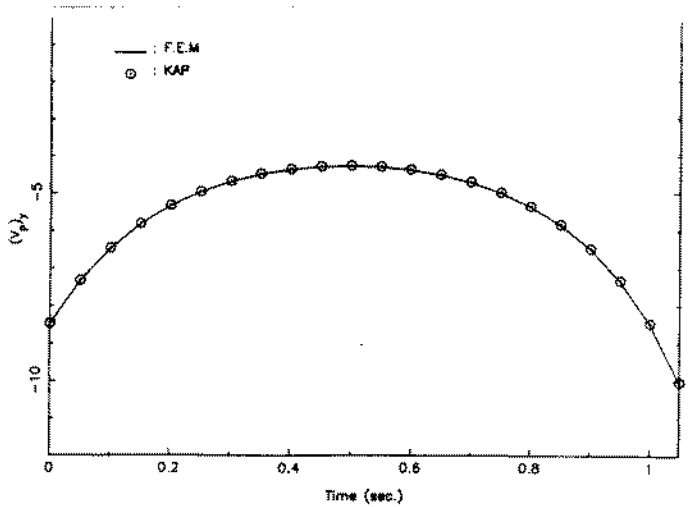

Fig. 14b- Peaucellier-Lipkin Mechanism- Time History of the Velocity of Point P

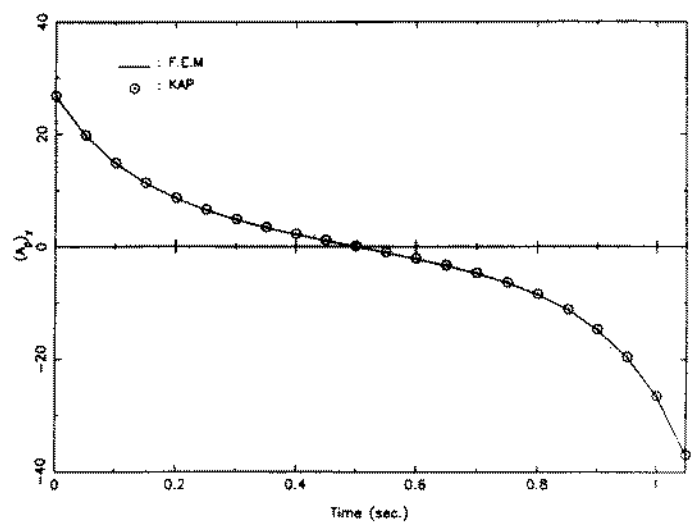

Fig. 14c- Peaucellier-Lipkin Mechanism- Time History of the Acceleration of Point P

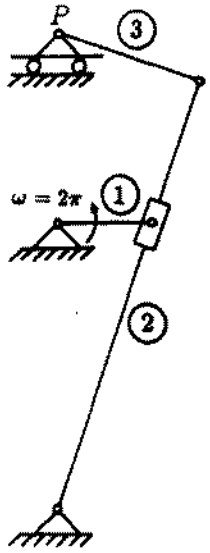

Fig. 15- Quick Return Mechanism

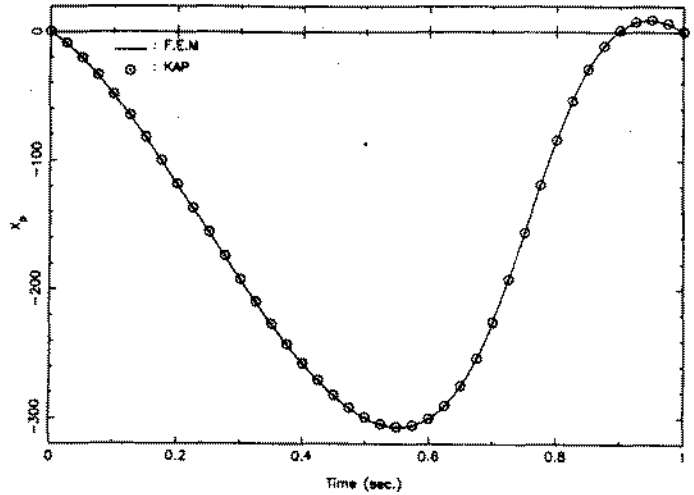

Fig. 15a- Quick Return Mechanism- Time History of the Position of Point P

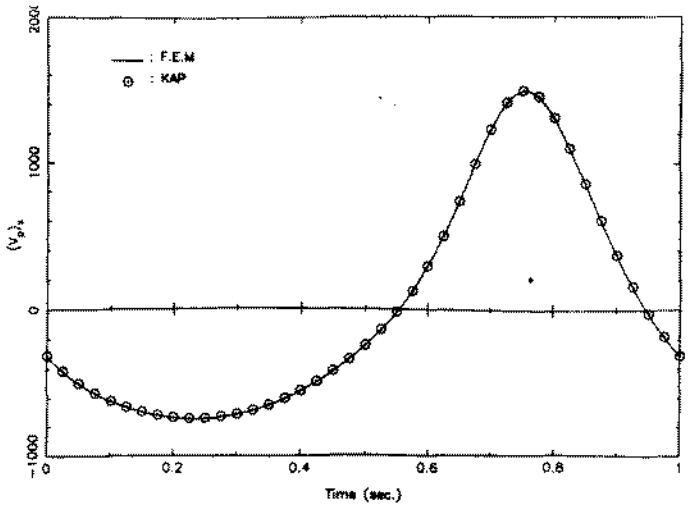

Fig. 15b- Quick Return Mechanism- Time History of the Velocity of Point P

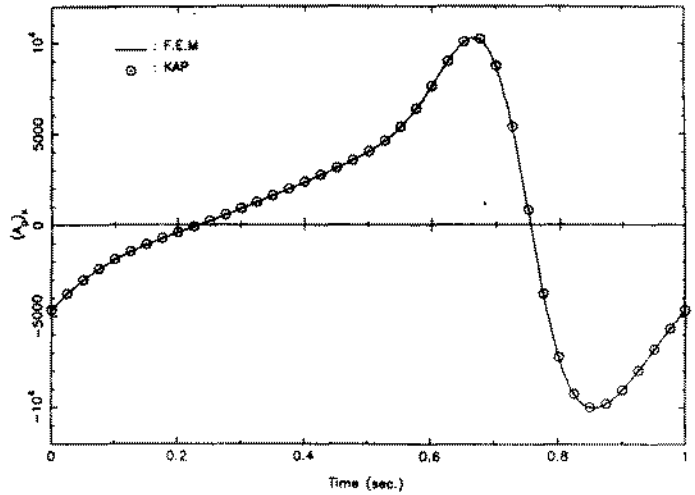

Fig. 15c- Quick Return Mechanism- Time History of the Acceleration of Point P